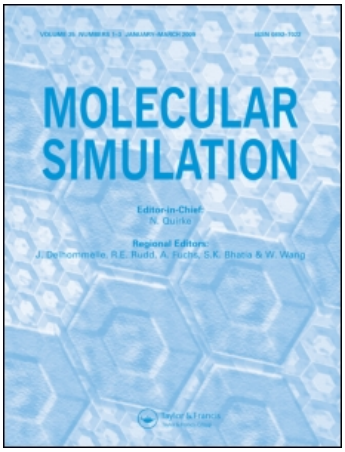

Molecular Simulation
Publication details, including instructions for authors and subscription information:
http://www.informaworld.com/smpp/title~content=t713644482

Simulation of Isoenthalps and Joule-Thomson Inversion Curves of Pure Fluids and Mixtures

Fernando A. Escobedo[a]; Zhong Chen[a]
[a] School of Chemical Engineering, Cornell University, Ithaca, NY

To cite this Article Escobedo, Fernando A. and Chen, Zhong(2001) 'Simulation of Isoenthalps and Joule-Thomson Inversion Curves of Pure Fluids and Mixtures', Molecular Simulation, 26: 6, 395 — 416
To link to this Article: DOI: 10.1080/08927020108024513
URL: http://dx.doi.org/10.1080/08927020108024513

Molecular Simulation, 2001, Vol. 26, pp. 395–416
Reprints available directly from the publisher
Photocopying permitted by license only

SIMULATION OF ISOENTHALPS AND JOULE-THOMSON INVERSION CURVES OF PURE FLUIDS AND MIXTURES

FERNANDO A. ESCOBEDO* and ZHONG CHEN

School of Chemical Engineering, Cornell University, Ithaca, NY 14853-5201

(Received May 2000; accepted July 2000)

This paper examines the molecular simulation of expansion and compression processes of fluids under common non-isothermal conditions. It is shown that accurate isoenthalps can be traced if simulated configurational properties obtained from the particular molecular force-field adopted are complemented by experimentally-based data for the ideal-gas contributions to the heat capacity. The simulation of inversion curves is also analyzed and found to be particularly challenging as conventional extrapolation techniques have limited applicability. Several approaches were investigated to overcome such difficulties including (1) simulation of several isobars and isoenthalps, (2) thermodynamic integration, and (3) histogram reweighting techniques. Contrary to the results of a recent study, our calculations show that the Johnson *et al.*, equation of state does provide a good description of the inversion curve for the Lennard-Jones fluid. Isoenthalps and the inversion curve for a model gas condensate mixture were also simulated; calculations of this sort could be used to identify conditions at which isoenthalpic decompression leads to heating of hydrocarbon reservoir fluids.

Keywords: Molecular simulation; Joule-Thomson; Isoenthalps

I. INTRODUCTION

The adiabatic throttling of gases plays a key role in processes for cooling and liquefying gases and for the operation of refrigeration devices [1]. As a gas is passed adiabatically through a contraction, the enthalpy (h) of the fluid remains constant; as a result, the gas temperature (T) will change as the pressure (P) drops (the Joule-Thomson effect). The suitable

*Corresponding author.

thermodynamic parameter that relates such changes of T and P is the Joule-Thomson (JT) coefficient μ_J:

$$\mu_J = \left(\frac{\partial T}{\partial P}\right)_h = \frac{1}{c_P}\left[T\left(\frac{\partial v}{\partial T}\right)_P - v\right] \tag{1}$$

where v and c_p are the specific volume and constant-pressure heat capacity, respectively. The sign of μ_J at any given condition will determine whether the gas is cooled ($\mu_J > 0$) or heated ($\mu_J < 0$) upon throttling. Because of this, liquefaction and refrigeration of gases by JT expansion may require that the system be preconditioned to a suitable thermodynamic region (*e.g.*, by precooling) so that μ_J is (sufficiently) positive. Gas expansions at nearly isoentropic conditions (*e.g.*, reversible-adiabatic turbines) are also important processes for liquefaction and refrigeration of fluids; in this case the suitable thermodynamic coefficient is given by:

$$\mu_K = \left(\frac{\partial T}{\partial P}\right)_s = \frac{T}{c_P}\left(\frac{\partial v}{\partial T}\right)_P \tag{2}$$

Because $\mu_K > \mu_J$ everywhere, isoentropic expansions are more efficient than isoenthalpic ones at cooling gases; however, isoenthalpic expansion operations are more ubiquitous due to their simplicity and low capital cost involved. The design and selection of new refrigeration fluids (whether pure compounds of multicomponent mixtures) will strongly depend on the shape of isoenthalps/isoentropes and the behavior of properties like μ_J and μ_K in the thermodynamic region of interest.

Besides their importance in refrigeration processes, isoenthalpic expansions play an important role in the exploitation and transport of hydrocarbon reservoir fluids. Modern techniques have enabled drilling operations at considerable depths where the oil sustains high pressures and temperatures. The release of gas from such a reservoir can be approximated by an isoenthalpic process; it is important in such processes to predict the effect of composition and reservoir conditions on the thermodynamic and transport properties of the gas. At pressure relief, temperature increases of the condensate have been observed in deep reservoirs [2], indicative of conditions at which the JT coefficient is negative.

For refrigeration/liquefaction process design and for reservoir engineering, it is important to have accurate tools to map out isoenthalps/isoentropes and to predict the conditions at which the Joule-Thomson coefficient changes sign. The locus of PT points that satisfy the condition that $\mu_J = 0$ is called the JT inversion curve. Several studies have provided

experimental data on isoenthalps and JT inversion points (see for example [3]). Unfortunately, the accuracy and availability of experimental data tends to diminish drastically near the inversion curve. Typically, numerous measurements of PVT data at difficult conditions are necessary to locate JT inversion points [6]. Equations of state (EoS) provide an alternative means to compute isoenthalps, PVT data, and JT inversion curves. It has been demonstrated in several studies, however, that EoS predictions tend to be particularly unreliable for calculation of JT inversion curves [4, 5]. There have been a few recent studies that have employed molecular simulation methods to estimate the JT inversion curve for the Lennard-Jones fluid [7–9] and for a model carbon dioxide fluid [10]. In the method of Heyes and Llaguno [7], the inversion points were found by mapping isoenthalps (by an approximate molecular dynamics scheme) and then locating the maximum of the P–T diagram (wherein $\mu_J = 0$). Colina and Muller used the fact that when $\mu_J = 0$, Eq. (1) leads to:

$$\left(\frac{\partial Z}{\partial T}\right)_P = 0 \tag{3}$$

where Z is the compressibility factor. Colina and Muller then conducted a series of simulations to map out several isobars (over a range of temperatures); each isobar was then fitted to a polynomial function of T [as either $v = v(T)$ or $Z = Z(T)$] which was then differentiated to estimate the location of the extrema points.

Just as with experimental measurements, however, JT inversion points are difficult to measure by molecular simulation, particularly at high temperatures. The most accurate data to date for the Lennard-Jones fluid appear to be those of Colina and Muller [8]. Their results indicate that none of the EoS available provides a good fit to the simulated Lennard-Jones JT inversion points. In particular, they found that the Johnson *et al.* EoS [11], whose parameters where fitted to extensive Lennard-Jones fluid simulation data, does not provide a good description but for a limited portion of the simulated JT inversion curve [9].

To the best of our knowledge, the Heyes and Llaguno work is the only study that has reported simulated isoenthalps (of a Lennard-Jones fluid) [7]. The first objective of this work is to explore the ability of united-atom force fields to accurately map isoenthalps (and isoentropes) of specific compounds. This is a non-trivial issue since enthalpy-related quantities strongly depend on the intramolecular degrees of freedom, many of which are missing in a classical united-atom model. It is shown here that the

incorporation of substance-specific ideal-gas heat capacity information into the simulation provides a practical means to obtain accurate isoenthalps. Methane, nitrogen, and hydrocarbon mixtures are used as testbeds for these calculations. The second objective of this work is to revisit the methodology for the simulation of JT inversion curves for simple fluids and mixtures. A two-step method is proposed here that comprises (i) the sequential mapping of an "approximate" inversion curve through an integration method wherein the predictor steps are aided by a EoS that is (piecewise) parameterized with simulation data, and (ii) the refinement of selected JT inversion data (from the first step) through a series of isobaric simulations as in the method of Colina and Muller [8] but within a multihistogram-reweighting [12] parallel-tempering scheme [13–15]. The proposed method is employed to simulate the inversion curve of the Lennard-Jones fluid, nitrogen, and of a model seven-component gas condensate mixture. It is shown that, in contrast to what was concluded in previous simulation studies, the Johnson *et al.*, BoS predictions are in good agreement with our simulated Lennard-Jones fluid inversion curve.

The rest of the paper is organized as follows. In Section II we present the methodology and the results relevant to the simulation of isoenthalps. In Section III we present the methodology and the results for the calculation of JT inversion curves. Finally in Section IV, we provide a few concluding remarks.

II. ISOENTHALPS

II.1. Methodology

It is in principle straightforward to numerically integrate Eqs. (1) or (2) to trace an isoenthalp or an isoentrope, respectively. While there is some freedom regarding the ensemble type that can be used to do this, we adopt here isothermal–isobaric ensembles (NPT) because they are naturally suited to describe multicomponent mixtures of fixed compositions. For example, integration of Eq. (1) can be performed by starting at an initial point (T_o, P_o) lying on the desired isoenthalp (with enthalpy h_{ref}), then if a pressure change ΔP is preset, the temperature for the new state can be extrapolated from a simple Euler scheme:

$$\Delta T \approx \mu_J^o \Delta P = \left[\frac{T(\partial v/\partial T)_P - v}{c_P}\right]\Delta P \tag{4}$$

where the term in brackets is evaluated at the initial state (T_o, P_o). The "fluctuation" quantities needed to evaluate μ_j^o, such as $(\partial v/\partial T)_P$, and $c_P = (\partial h/\partial T)_p$ can be readily obtained during a NPT simulation [16]. Further, one could use a higher-order integration scheme (*e.g.*, predictor corrector schemes), or even better, a histogram reweighting technique [17, 12] to perform the extrapolations [18]. However, except for simple molecules and relatively small system sizes, histogram reweighting will not offer a significant advantage over simpler integration schemes [19]. Here a simple integration scheme is implemented based on a first-order Taylor-expansion around a simulation point (T_o, P_o):

$$h^{\text{ref}} = h^o + \left(\frac{\partial h}{\partial \beta}\right)_P \Delta\beta + \left(\frac{\Delta h}{\partial P}\right)_\beta \Delta P \tag{5}$$

where $\beta = (k_B T)^{-1}$ (k_B is Boltzmann constant); upon rearrangement:

$$\Delta\beta = \left[h^{\text{ref}} - h^o - \left(\frac{\partial h}{\partial P}\right)_\beta \Delta P\right] \Big/ \left(\frac{\partial h}{\partial \beta}\right)_P \tag{6}$$

Eq. (6) has the advantage [over Eq. (4)] of allowing a correction of the extrapolated temperatures when the measured enthalpy h_o does not match the reference value h^{ref}. In this scheme, simulations are never conducted on the isoenthalp but *close to* it; Eq. (6) can be used to extrapolate T for a new pressure point, or to refine T for the recently simulated state (*i.e.*, for $\Delta P = 0$).

A subtle point for the implementation of Eq. (6) or of any related extrapolation scheme, is the evaluation of enthalpies and heat capacities. The problem is that only the configurational part of such properties can be measured during a molecular simulation; for the extrapolations, however, the total properties are needed, *e.g.*, including the non-trivial ideal-gas contributions. In principle, one could evaluate such ideal-gas effects for the specific molecular model adopted (which may lack internal-vibrations and explicit hydrogen atoms); as it will be shown later, however, such an approach can lead to significant departures from realistic values. Consider instead the general problem of tracing an "iso-X" curve, wherein certain parameter "X" is to remain constant. Such a parameter can be seen as an arbitrary combination of measured properties (like the configurational enthalpy) and externally specified quantities or functions. If we choose X to be the best estimate of the enthalpy of the real system, then it is given by the sum of the simulated configurational contributions (extracted from simulation) and ideal-gas contributions as obtained from correlations of

experimental data [20]. For an articulated multi-site molecule, however, simulation does measure some portion of the ideal gas enthalpy; the suitable correction term can then be obtained from the simulated constant-volume heat capacity (c_V) of a single molecule in vacuum;

$$c^{ig}_{V_{\text{conf}}} = k_B\beta^2 \,\text{cov}(U_{\text{conf}}, U_{\text{conf}}) \tag{7}$$

where U_{conf} is the configurational intramolecular potential energy of the molecule (*e.g.*, the sum of bending potentials, torsional potentials, and intra site–site pair interactions), and "cov" denotes the covariance between two variables: $\text{cov}(y_i, y_j) = \langle y_i y_j \rangle - \langle y_i \rangle \langle y_j \rangle$ (where the "$\langle\rangle$" denote ensemble average).

Polynomial correlations for the ideal gas c^{ig}_P are readily available for most known fluids [21]; these are based on experimental data and account for all ideal-gas contributions to c_P including translational, rotational, and vibrational motions (in addition to non-bonded interactions). Figure 1 shows a comparison between experimentally-based $c^{ig}_V = c^{ig}_P - R$ (where R is the gas constant) and simulated $c^{ig}_{V_{\text{conf}}}$ for a few normal alkanes; the force field from Ref. [22] (where methylene and methyl groups are described as Lennard-Jones sites) was used for these calculations; torsional and bending

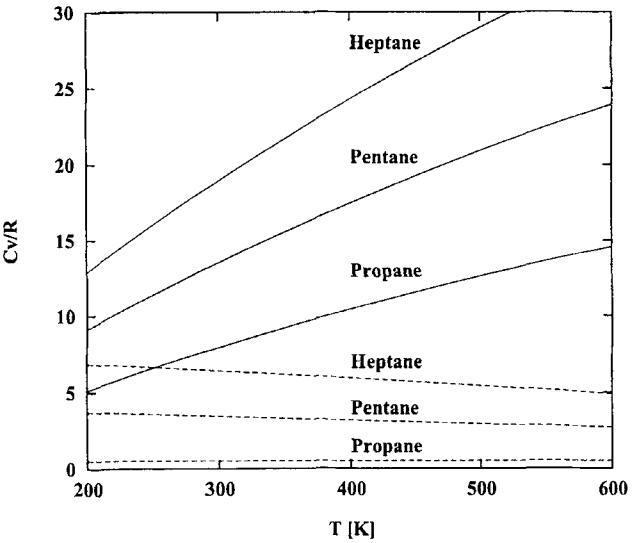

FIGURE 1 Constant volume heat capacities c^{ig}_V for the ideal gas state of propane, pentane, and heptane. The full lines show c^{ig}_V from polynomial correlations based on experimental measurements [21]; the dashed lines show the "configurational" contribution to c^{ig}_V as obtained from simulation of the united-atom force field of Ref. [22].

potentials are included but bond lengths are fixed at their equilibrium values. For such models, methane and ethane have $c^{ig}_{V_{\text{conf}}} = 0$. Note in Figure 1 that, for any given alkane, $c^{ig}_{V_{\text{conf}}}$ is only a small fraction of c^{ig}_V; also, c^{ig}_V increases monotonically with temperature while $c^{ig}_{V_{\text{conf}}}$ exhibits the opposite trend.

At any given temperature T_o, the quantity $h^{\text{ref}} - h^o$ needed in Eq. (6) can then be evaluated from:

$$h^{\text{ref}} - h^o = h^{\text{ref}}_{\text{conf}} - h^o_{\text{conf}} + h^{ig'}_{\text{ref}} - h^{ig'}_o \tag{8}$$

where h_{conf} is the configurational enthalpy, and $h^{ig'}$ is the portion of the ideal-gas enthalpy that is not in the configurational part, *i.e.*,

$$h^{ig'} = h^{ig} - h^{ig}_{\text{conf}}$$

thus Eq. (8) becomes

$$h^{\text{ref}} - h^o = h^{\text{ref}}_{\text{conf}} - h^o_{\text{conf}} + \int_{T_o}^{T_{\text{ref}}} [c^{ig}_V - c^{ig}_{V_{\text{conf}}}] dT \tag{9}$$

Likewise, the term $(\partial h/\partial\beta)_P$ needed in Eq. (6) follows from Eq. (9):

$$\left(\frac{\partial h}{\partial \beta}\right)_P = -\frac{c_P}{k_B\beta_o^2} = -\frac{1}{k_B\beta_o^2} c_{P_{\text{conf}}} - \frac{1}{k_B\beta_o^2}[c^{ig}_V - c^{ig}_{V_{\text{conf}}}] \tag{10}$$

where $c_{P_{\text{conf}}} = k_B\beta_o^2 \text{cov}(U + PV, U + PV)$ and U is the configurational internal energy that includes intramolecular and all intermolecular interactions. The term $(\partial h/\partial P)_\beta$ in Eq. (6) does not require any special treatment since it only depend on volumetric properties [*i.e.*, $(\partial h/\partial P)_\beta = v + \beta(\partial v/\partial\beta)_P$].

II.2. Simulations

The first step for this type of studies should be the identification of the vapor–liquid phase envelope because isoenthalpic simulations will be different depending on the number of phases present. In Ref. [23], a formalism based on the pseudo-ensemble method has been presented for both: (1) locating the phase envelope of the system (*e.g.*, the dew line for a gas mixture) and (2) simulating isoenthalpic diagrams within the two phase region (isoenthalpic flash calculations). The reader is referred to such a

reference for details on these methods; for the ensuing discussion, simulations are restricted to the one-phase vapor or supercritical-fluid region.

Methane provides a simple example to examine the importance of ideal-gas effects on the simulation of isoenthalps. The methane united-atom model adopted here [24] is a fluid of Lennard-Jones spheres; its "actual" $c_V^{ig}(\text{model}) = (3/2)R$ (R is the gas constant) is significantly different from the experimentally based $c_V^{ig}(\text{exp})$. Simulations were carried out to trace isoenthalps *via* iterative use of Eq. (6) with either $c_V^{ig}(\text{model})$ or $c_V^{ig}(\text{exp})$; these runs employed 500 molecules and 5×10^4 cycles/point. The results of these simulations are shown in Figure 2; clearly, the use of $c_V^{ig}(\text{exp})$ leads to isoenthalps that agree much better with experimental data.

Figures 3 and 4 show isoenthalps for nitrogen (force field from [25]) and for a model condensate mixture composed of methane (74.2 mole %), ethane (10.0%), propane (5.0%), butane (3.0%), pentane (1.2%), hexane (1.0%) and heptane (5.6%) [26]. The nitrogen simulations employed 400 molecules and the condensate simulations employed 600 molecules. A total of $4-6 \times 10^4$ Monte Carlo cycles [16] per state point (or integration step) were employed. Thermal equilibration was accomplished through a combination of translation, rotation, reputation, and configurational-bias

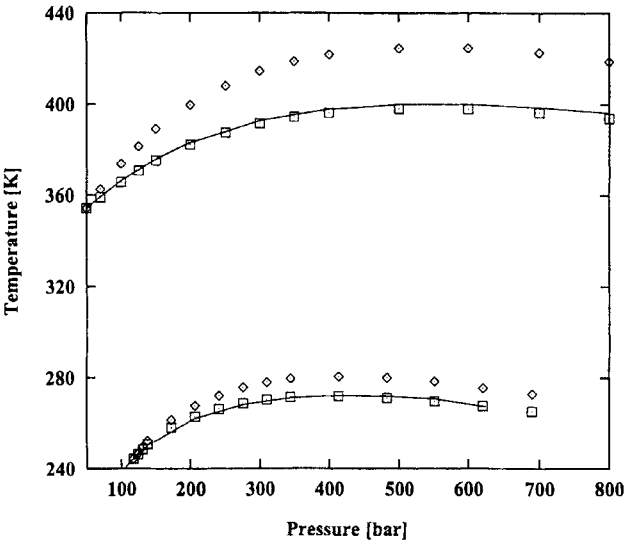

FIGURE 2 Isoenthalps for methane. Interpolations based on experimental data [39] are shown by full lines. The simulation results for the force field of Ref. [24] are presented when c_V^{ig} for monoatomics is used (diamonds), and when c_V^{ig} for methane [21] is used (squares). For each isoenthalp, the starting point for the thermodynamic integration is the point at the lowest pressure. Errorbars of simulation data are smaller than the symbol sizes.

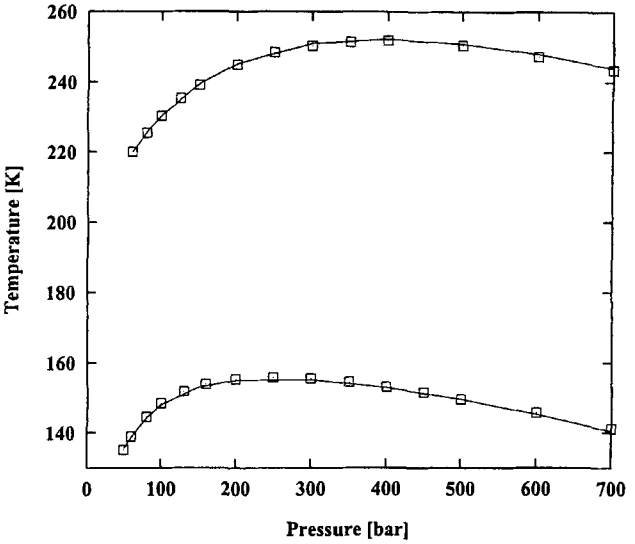

FIGURE 3 Isoenthalps for Nitrogen. Interpolations based on experimental data [39] are shown by the full lines. Simulation data are shown by squares; these use c_V^{ig} data for nitrogen from [21]. The integration series for the high temperature isoenthalp was the point at $P = 60$ bar and for the low-temperature isoenthalp was the point at $P = 500$ bar. Errorbars of simulation data are smaller than the symbol sizes.

moves [27, 28]. A cutoff radius of 11 Å was employed for Lennard-Jones interactions and standard tail corrections were implemented; for unlike pair interactions, the standard Lorentz-Berthelot combining rules were employed [16]. For the alkanes, the potential models for methane, ethane, and propane-and-longer alkanes are from Jorgensen *et al.* [24], Spyriouni *et al.* [29] and Nath *et al.* [22], respectively.

For the three systems examined in Figures 2–4, the JT inversion point is clearly evidenced as the maxima in the curves. These inversion points lie on the low-temperature branch of the JT inversion curve. As for the case of methane, the isoenthalps of nitrogen agree well with experimental data. Experimental data are not available for the model gas condensate; however, since the majority component is methane, experimental and simulated curves for pure methane are given for comparison. Methane and the gas condensate are both expanded from the same initial state: 400 K and 1000 bar. The presence of heavy alkanes in the gas condensate has the net effect of increasing the temperature raise upon decompression; this is in agreement with the analysis of gas condensates *via* EoS by Kortekaas *et al.* [30]. Note that the lowest-pressure point lies near the dew-point boundary of the gas condensate. It should be pointed out that despite the overall good

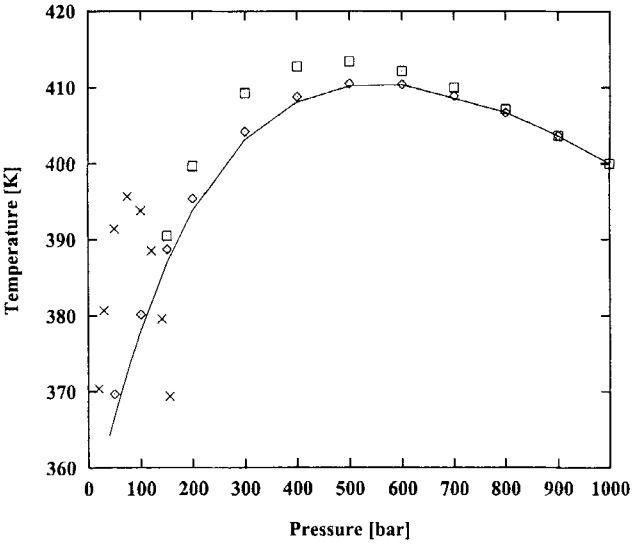

FIGURE 4 Isoenthalp for a seven-component gas condensate (squares); composition: methane 74.2 mole %, ethane 10.0%, propane 5.0%, butane 3.0%, pentane 1.2%, hexane 1.0% and heptane 5.6%. The gas condensate dew-line, depicted by the crosses, encircles the two-phase region and was obtained as described in Ref. [23]. Results are also shown for the isoenthalpic expansion of methane starting at the same initial state ($P = 1000$ bar and $T = 400$ K); simulation data are shown by diamonds and experimental data (based on Ref. [39]) are shown by a full curve. Errorbars of simulation data are commensurate to size of the symbols.

agreement between simulated and experimental isoenthalps, the flatness of the curves near the maxima precludes an accurate estimate of the JT inversion point.

Although our discussion has been restricted to the calculation of isoenthalps, the simulation of isoentropes based on Eq. (2) can be carried out in a completely analogous manner.

III. JOULE-THOMSON INVERSION CURVES

III.1. Methodology

JT inversion curves could be found by tracing numerous isoenthalps such as those shown in Figures 2–4; it should be noted, however, that the location of inversion points is independent of the ideal-gas contributions to the enthalpy. Alternatively, JT inversion curves can be obtained by tracing numerous isobars as in the method of Colina and Muller [8]. However, unless we are interested in the isoenthalps or isobars themselves, a more

efficient approach should try to concentrate the simulations near the inversion curve. It is instructive to write an equation whose integration would lead to a stepwise simulation of the JT inversion curve. For example, expanding the compressibility factor in a Taylor series around a point (T_o, P_o):

$$Z = Z_o + Z_P^o \Delta P + Z_\beta^o \Delta\beta + \frac{1}{2} Z_{\beta\beta}^o \Delta\beta^2 + \frac{1}{2} Z_{PP}^o \Delta P^2 + Z_{\beta P}^o \Delta\beta \Delta P \tag{11}$$

where for brevity we write $Z_P = (\partial Z/\partial P)_\beta$, $Z_\beta = (\partial Z/\partial\beta)_P$, and similar conventions for the second order derivatives. For a preset $\Delta\beta$, a neighboring JT inversion point must satisfy $Z_\beta = 0$ which leads to:

$$\Delta P = -\frac{Z_\beta^o - Z_{\beta\beta}^o \Delta\beta}{Z_{\beta P}^o} \tag{12}$$

the equivalent result when volume is expanded in a Taylor-series based on the Quasi-gaussian entropy theory [32, 33] is (see the Appendix):

$$\frac{P_o}{P} = 1 + \frac{v_T^o T_o - v_o + v_{TT}^o T_o (T - T_o)}{T_o P_o v_{TP}^o - P_o v_P^o} \tag{13}$$

In contrast to common integration schemes, like Eq. (6) or Gibbs-Duhem integration methods [34], Eqs. (12) or (13) require knowledge of second order derivatives (*i.e.*, third order moments of the ensemble density distribution function). While such derivatives can be readily estimated *via* fluctuation formulas (from data collected at the previous point), or *via* finite difference expressions (from data of several previous points), the statistical noise tends to be prohibitively large. Attempts of using Eqs. (12), (13) and similar variants were mostly fruitless because quite accurate values of first- and higher-order derivatives are needed to obtain reasonably accurate results (even for the simple case of the Lennard-Jones fluid). Single histogram reweighting calculations (equivalent to infinite-order Taylor expansions) were useful only for very short extrapolations and provided very long runs were conducted (*e.g.*, over 2×10^5 cycles). Multiple histogram reweighting, even when used with small system sizes (200 Lennard-Jones spheres) and combined with multidimensional parallel tempering [14, 15] improved only marginally the accuracy of the results. Numerical problems are particularly severe near the maximum-pressure region and for high temperatures.

As it will be shown later, even first-order moments cannot be simulated with sufficient precision to accurately locate inversion points in certain

regions. We attempted several approaches to produce extrapolations based on first- and (at most) second-order simulated moments which did not diverge uncontrollably. One approach that showed good stability is based on piecewise fitting of an equation of state (EoS) to simulation data. A cubic EoS is employed to illustrate the idea; for concreteness, a generalized three-parameter Redlich-Kwong EoS is adopted [31]:

$$P = \frac{RT}{v-b} - \frac{aT^{-\alpha}}{v(v+b)} \tag{14}$$

where a, b and α are the three fitting parameters. Although these parameters are usually evaluated from substance-specific critical parameters and acentric factors; for our purposes however, they are seen as adjustable constants to be locally fitted to simulation data. For example, if at a given simulation point (P_o, T_o) we evaluate v_o, $v_T^o = (\partial v/\partial T)_P$, and $v_P^o = (\partial v/\partial P)_T$, then it can be shown that parameters b, α and a can be found from:

$$1 + \frac{RT_o v_P^o}{(v_o-b)^2} - \left(\frac{RT_o}{v_o-b} - P_o\right)\frac{(2v_o+b)v_P^o}{v_o(v_o+b)} = 0 \tag{15}$$

$$\alpha = \frac{(T_o v_T^o/(v_o-b)) - 1}{1 - (P_o(v_o-b)/RT_o)} - \frac{(2v_o+b)T_o v_T^o}{v_o(v_o+b)} \tag{16}$$

$$a = T_o^{\alpha}\left(\frac{RT_o}{v_o-b} - P_o\right)v_o(v_o+b) \tag{17}$$

Alternatively, the three parameters can be found by non-linear fitting to the results of more than one point; for most of our calculations two points were used. Once a, b and α are known, a neighboring inversion point for a given T can then be found from Eq. (14) and:

$$T^{\alpha+1} = \frac{a}{bR}\left(\frac{v-b}{v+b}\right)^2\left[\frac{\alpha(v+b)+2v+b}{v}\right] \tag{18}$$

The proposed method can be seen as an example of a hybrid technique that combines simulation data and an engineering model in an attempt to harness the predictive capabilities of the former with the economy and extrapolative capability of the latter. However, because the analytical

model employed may introduce some systematic deviations into the results, selected inversion points should be checked and refined with independent simulations. For this reason, the following sequential approach is suggested:

- Locate first a point on the inversion curve, this can be achieved by either tracing an isoenthalp or an isobar at a relatively low temperature.
- Map out, point by point, an approximate inversion curve (through temperature changes) wherein the position of the next point is found with an EoS whose parameters have been fitted to simulation data.
- As new (approximate) inversion points are simulated, the location of former points can be refined based on improved piecewise parameterization of the EoS.
- Once the desired portion of the "approximate" inversion curve has been generated; selected points along the curve are refined through a series of isobaric simulations whose results are then extrapolated by a multi-histogram-reweighting technique [12, 15].

III.2. Simulations

Inversion curves were traced for the Lennard-Jones fluid, a model nitrogen fluid (force-field from [25]) and a model gas condensate mixture (whose composition and potential model are the same as those used before for the isoenthalpic expansion reported in Fig. 4). Both a 200-molecule system and a 500-molecule system were investigated for the Lennard-Jones fluid (the smaller system facilitates the analysis of data through the histogram reweighting technique). A 400-molecule system was employed for nitrogen and a 600-molecule system for the gas condensate. All simulations were conducted in the NPT ensemble following the methodological details described before for tracing isoenthalps.

The results for the Lennard-Jones fluid are shown in Figures 5 and 6. A first inversion point for $T^* = Tk_B/\varepsilon = 1.9$ was located by using the simulated low-temperature methane isoenthalph of Figure 2. From that point, two stepwise "approximate" EoS-aided extrapolations were conducted, one for decreasing temperatures, and another for increasing temperatures with $\Delta T^* \sim 0.135$ (using $\sim 10^5$ cycles/point). For comparison, the JT inversion curve obtained from the Johnson *et al.*, EoS [11] and the simulation data of Colina and Muller [8] are also shown. In spite of the relatively large statistical noise of our results for $T^* > 2.0$, they agree better with the EoS curve than with Colina and Muller's data. Our data and Colina and Muller's

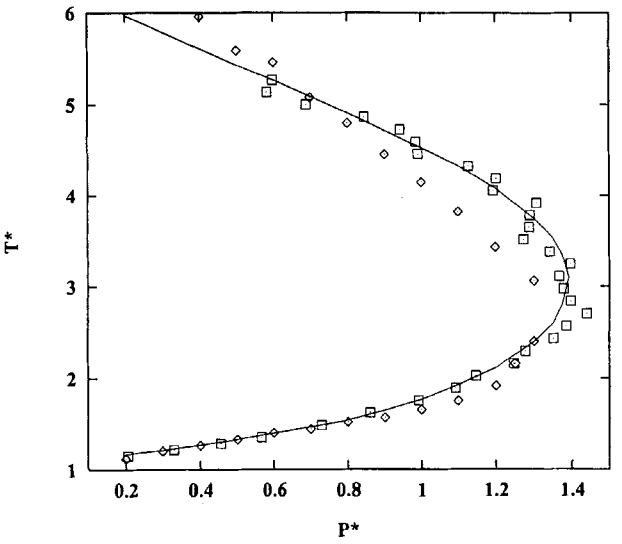

FIGURE 5 Inversion curve for the Lennard-Jones fluid ($T^* = Tk_B/\varepsilon$ and $P^* = P\sigma^3/\varepsilon$); predictions from the Johnson *et al.*, EoS [11] are shown by the full line, simulation data from Colina and Muller [8, 9] are shown by diamonds, and our simulation data ("approximate" inversion curve) are shown by squares. Errorbars for our simulation data are commensurate to the symbol size for $T^* < 2$ but they grow up to order ± 0.1 units of P^* for larger T^*.

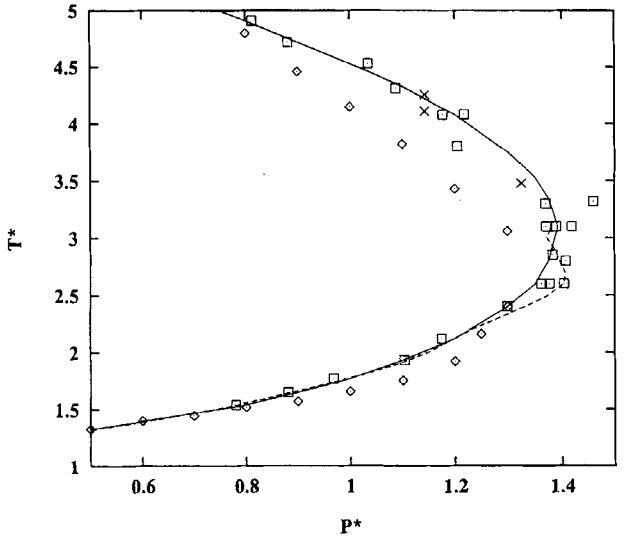

FIGURE 6 Inversion curve for the Lennard-Jones fluid; predictions from the Johnson *et al.*, EoS [11] are shown by the full line, simulation data from Colina and Muller [8, 9] are shown by diamonds, and extrapolations based on single-histogram reweighting are shown by squares. Results from a multi-histogram reweighting scheme are shown by the dashed lines; note that these extrapolations become irregular for $T^* > 2.2$. Estimated inversion points obtained by locating the maximum in Z *vs.* T isobars (like those in Fig. 7) are shown by the crosses.

data agree well for $T^* < 1.5$; systematic differences are observed even in the $1.5 < T < 2.0$ range where the errorbars of our simulation results are still moderate.

The reason why simulation data are more accurate for lower T^* (say, $T^* < 2$) is because isoenthalps are not as flat as at higher temperatures; this is a general feature that can be observed in Figures 2 and 3. We found that even extrapolations based on Eq. (13) (which require third-order moments) were feasible for $T^* < 2$. Once the approximate inversion curve was outlined, longer runs (2×10^5 cycles) with smaller systems (200 molecules) were performed using a parallel tempering scheme [13, 15]; histograms of energy and volume were then collected and analyzed by multi-histogram reweighting [12]. Some of the results are shown in Figure 6. These calculations did not improve significantly the accuracy of the data; reliable extrapolations were obtained for $T^* < 2.1$, but for higher T^* reweighting either failed to converge or led to non-reproducible outcomes. The results for $T^* > 4.2$, whenever reweighting converged, were consistent with the "approximate" curve found first.

The inversion-curve region between $T^* = 2.5$ and $T^* = 4.2$ is the most difficult to resolve and it is also where Colina and Muller's data and ours differ the most. Additional simulations were performed employing Colina and Muller's method at two pressures, $P^* = P\sigma^3/\varepsilon = 1.143$ and $P^* = 1.325$ (2×10^5 cycles/point) but employing parallel tempering (to improve ergodicity) and multihistogram reweighting analysis. The resulting Z *vs.* T curves are shown in Figures 7a and b; the estimated inversion points are shown in Figure 6. At $P^* = 1.143$ an inversion point (the maximum) is located at $T^* \approx 4.1$ (a similar calculation for a 360-molecule system gave $T^* \approx 4.2$); histogram reweighting nicely smoothes out the scatter in the single-point averages of Z. At $P^* = 1.325$, however, reweighted values of Z (which incorporate information from higher moments of all neighboring points) do not provide a good "fit" to the single-point averages (which only depend on the first-moment of volume at the specific point). The standard deviation of single-point Z values estimated from block averages during the run look enormous in the figure, but they are actually less than 0.1% (see the narrow scale of the y-axis). A value of $Z = 1.2137 \pm 0.0008$ would be sufficiently accurate for most applications, but it is not so for this calculation. Figure 7b indicates an inversion temperature of $T^* \approx 3.47$; the result from a second series of runs was $T^* \approx 3.53$, thus we estimate the inversion point to be $T^* = 3.5 \pm 0.06$. We conclude that the Lennard-Jones inversion curve near the maximum-pressure is in good agreement with the Johnson *et al.*, EoS predictions and is inconsistent with the simulation

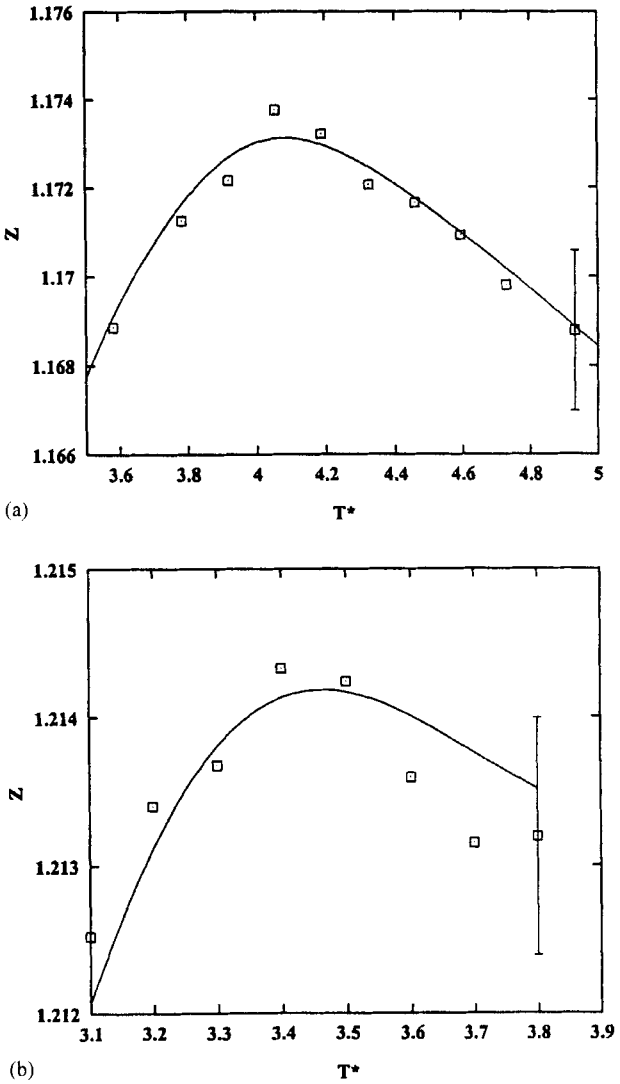

FIGURE 7 Compressibility factor as a function of temperature for the Lennard-Jones fluid for $P^* = 1.143$ (top) and $P^* = 1.325$ (bottom). Squares are the average values evaluated at the actual simulated point and the lines are the results based on multi-histogram reweighting of all simulation points. The typical standard deviation for single-run averages is depicted for the rightmost point.

results of Colina and Muller. We speculate that the main reason why Colina and Muller's results do not always agree with ours is that their runs were too short. They typically used 10^4 cycles (to collect averages) per point while we

used runs at least 10 times longer. Other sources of discrepancy may be the differences in systems sizes and potential cutoff employed.

Figure 8 shows a portion of the inversion curve for nitrogen (force field from Ref. [25]); the starting point was obtained from the low-temperature isoenthalp of Figure 3. As with the Lennard-Jones fluid, the low temperature region is relatively easy to map out (*e.g.*, for $T < 180\,\mathrm{K}$) but as the pressure maxima is approached, the statistical noise becomes very large and the data no longer follow a smooth trend. Isobaric Z *vs.* T data were obtained at $P = 365$ bar to confirm the shape of the inversion curve in the high-pressure region. In spite of the significant statistical noise of our results, simulation data do seem to agree reasonably well with an inversion-curve that was fitted to experimental data [35].

Figure 9 shows the "approximate" inversion curve for the seven-component gas condensate used before (see Fig. 4); the starting point for the stepwise mapping was obtained from the isoenthalp of Figure 4. The inversion curves predicted using the Soave-Redlich-Kwong (SRK) EoS [36] and the Peng-Robinson (PR) EoS [37] are also shown for comparison (using conventional van der Waals mixing rules with zero binary interaction

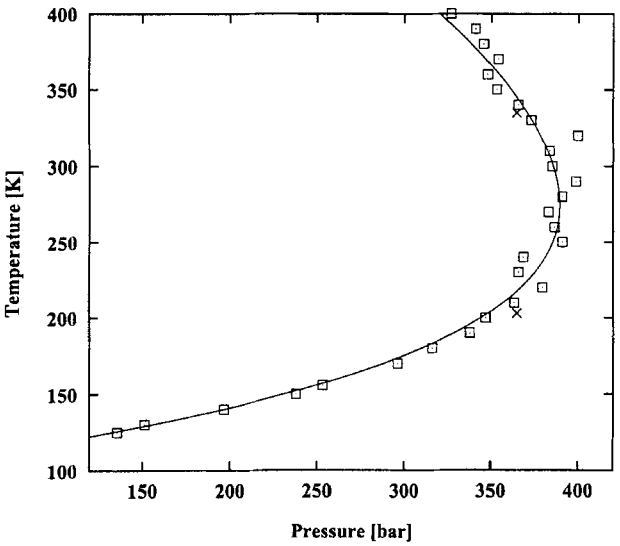

FIGURE 8 Inversion curve for nitrogen; the full line corresponds to a fit to experimental data [35]. The squares correspond to the "approximate" inversion curve from a EoS-aided thermodynamic integration; errorbars are commensurate to the symbol size for $T < 180\,\mathrm{K}$; they increase up to order ± 15 bars at higher temperatures. The crosses are inversion points calculated *via* the Colina and Muller method [8]; errorbars are estimated to be $\pm 9\,\mathrm{K}$.

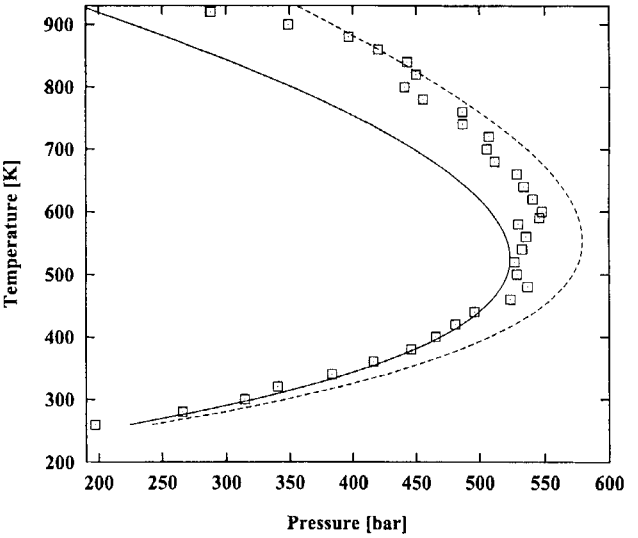

FIGURE 9 Inversion curves for the model gas condensate of Figure 4. The squares correspond to simulation data; the full and dashed lines correspond to the predictions of the Soave-Redlich-Kwong EoS [36] and the Peng-Robinson EoS [37], respectively. Errorbars of simulation data are commensurate to the symbol size for $T < 180$; they increase up to order $\pm$ 18 bars at higher temperatures.

coefficients [21]). Simulation results lie in between the two EoS curves; they are closer to the SRK EoS inversion curve for $T < 430$ K but they are closer to the PR EoS inversion curve for $T > 700$ K. This behavior is qualitatively consistent with that observed when experimental inversion curves of simple fluids are compared to the predictions of these two EoS [4]: the SRK EoS curve agrees well with the low-temperature branch of the inversion curve but underestimates the inversion pressure at higher temperatures, while the PR EoS tends to overestimate the inversion pressure at all temperatures. Figure 10 shows a comparison between simulated and SRK inversion data for the model gas condensate of Figure 9 and for pure methane (the majority component in the gas condensate). It is observed that the net effect of "heavies" in the gas condensate is that of shifting the curve to higher temperatures; this effect is qualitatively captured by the EoS. For methane, simulation data and experimental data agree well. Although no experimental data is available for the model gas condensate; it can be argued, based on the observations given above, that our simulation data must provide a more reliable prediction of the inversion curve than any of the two EoS tested here.

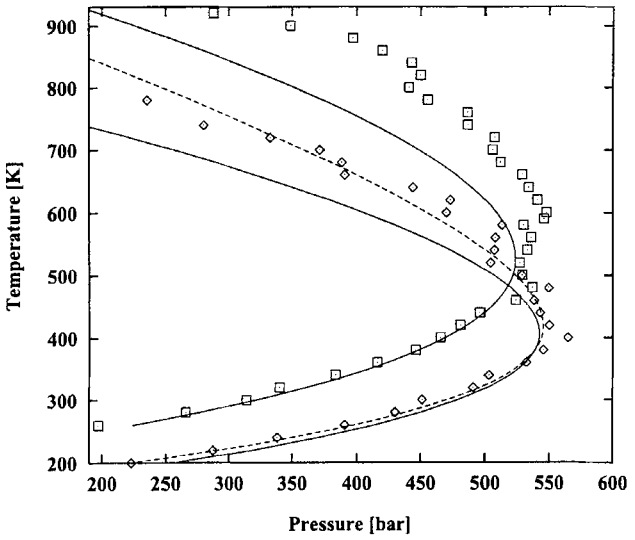

FIGURE 10 Inversion curves for a model gas condensate of (same as in Fig. 9) and for methane. The squares correspond to simulation data, the full line corresponds to the predictions of the Soave-Redlich-Kwong EoS [36], and the dashed line corresponds to "experimental" results as given by a correlation from Ref. [5].

IV. CONCLUDING REMARKS

This work presents novel methods for tracing isoenthalps, isoentropes, and inversion curves for single fluids and mixtures by molecular simulation. These calculations can be employed for the development of new refrigerant mixtures provided that good force fields can be constructed. The ability to simulate these properties can also be of value for the engineering of flow processes involving reservoir fluids. To illustrate the usefulness of the proposed methods, several systems have been studied including the Lennard-Jones fluid, nitrogen, and a model seven-component gas condensate.

It has been shown that fairly accurate isoenthalps (and isoentropes) can be traced with simple united-atom potential models provided that accurate ideal gas heat capacity data, c_V^{ig}, be used to complement the simulated configurational properties. The requirement of knowing c_V^{ig} is not necessarily a severe constraint for the application of this approach to "new" compounds; c_V^{ig} could be estimated by using quantum mechanical techniques and even by using group contribution methods with errors less than 1–2% [21].

A distinctive feature of the method proposed here for tracing inversion curves is that it relies on information of first- and higher-order moments of

the probability density function to extrapolate PVT data. Such information can be utilized by resorting to a histogram reweighting scheme or by employing a stepwise EoS parameterization approach. It has been found that accurate simulation of inversion points at high temperatures requires simulated averages with standard deviations smaller than 0.1%. This is a stringent challenge to any molecular simulation methodology and very long runs should be performed to obtain reproducible results.

While the isobaric–isothermal (NPT) ensemble adopted in this work appears to be the natural choice to perform JT inversion-curve simulations, other ensembles, like the grand canonical ensemble, could be more efficient by generating more accurate results for a given allocated computer time. This is because (grand canonical) insertion–deletion moves can sample the density and the energy fluctuations of low-density fluids more efficiently than NPT volume moves; volume moves are also very expensive. Grand canonical simulations, however, will not be as convenient to use with mixtures since compositions can not be fixed *a-priori*.

In view of the discrepancies found between our results and those of Colina and Muller for the inversion curve of the Lennard-Jones fluid, the recent results for the inversion curve of a model CO_2 reported by Chacin *et al.* [10] may need to be regarded with some caution; their results (using the Colina and Muller's method) support the existence of an unusual change of slope in the high-temperature branch of the inversion curve, where the statistical uncertainty tends to be prohibitively large.

APPENDIX: APPROXIMATE EXTRAPOLATION FORMULA

Berendsen *et al.*, have developed several variants of the so-called quasi-Gaussian entropy theory [32, 33, 38] for both canonical and noncanonical ensembles. For an isobaric–isothermal ensemble and within the diverging Gamma state, these authors provide the following "equation of state" extrapolation formulas based on the properties measured at a point "0"; at constant pressure:

$$v = v_o + v_T^o(T - T_o) + v_{TT}T_o\left[T\ \ln\left(\frac{T}{T_o}\right) - T + T_o\right] \tag{19}$$

and at constant temperature:

$$v = v_o - P_o^2 v_P\left(\frac{1}{P} - \frac{1}{P_o}\right) \tag{20}$$

where for brevity we write $v_P=(\partial v/\partial P)_T$, $v_T=(\partial v/\partial T)_P$, and $v_{TT}=(\partial^2 v/\partial T^2)_P$. Although no similarly simple equations have been derived for the situation when both temperature and pressure change, we can generalize the results above by noting that Eq. (19) is approximated a second-order Taylor expansion of v in T, and that Eq. (20) is a first-order Taylor expansion of v in P^{-1}; thus we could write:

$$v = v_o + v_T^o(T - T_o) + v_{TT}T_o\left[T\ln\left(\frac{T}{T_o}\right) - T + T_o\right] - P_o^2 v_P\left(\frac{1}{P} - \frac{1}{P_o}\right) - P_o^2 v_{TP}^o\left(\frac{1}{P} - \frac{1}{P_o}\right)(T - T_o) \tag{21}$$

If point (P, v, T) is an inversion point then Eq. (21) can be used to eliminate v by satisfying the inversion point condition, $Tv_T - v = 0$; the resulting relationship between P and T is Eq. (13) presented in Section III.

References

[1] Kyle, B. G., *Chemical and Process Thermodynamics*, Prentice Hall, 3rd edn., New Jersey, 1999.

[2] Baker, A. C. and Price, M., *SPE European Conference*, 21–24 October, 1990, pp. 217–230.

[3] Perry, R. H., Green, D. W. and Maloney, J. O., Editors, *Perry's Chemical Engineers' handbook*, McGraw-Hill, New York, 1984, pp. 3–107.

[4] Dllay, G. W. and Heldemann, R. A. (1986). "Calculation of Joule-Thomson inversion curves from equations of state", *Ind. Eng. Chem. Fundam.*, **25**, 152.

[5] Hendricks, R. C., Peller, I. C. and Baron, A. K. (1972). "Joule-Thomson inversion curves and related coefficients for several simple fluids", NASA TN D-6807.

[6] Roebuck, J. R. and Osterberg, H. (1935). "The Joule-Thomson effect in nitrogen", *Phys. Rev.*, **48**, 450.

[7] Heyes, D. M. and Llaguno, C. T. (1992). "Computer simulation and equation of state study of the Boyle and inversion temperature of simple fluids", *Chem. Phys.*, **168**, 61.

[8] Colina, C. M. and Muller, E. A. (1997). "Joule-Thomson inversion curves by molecular simulation", *Molecular Simulation*, **19**, 237.

[9] Colina, C. M. and Muller, E. A. (1999). "Molecular simulation of Joule-Thomson inversion curves", *Int. J. Thermophys.*, **20**, 229.

[10] Chacin, A., Vasquez, J. M. and Muller, E. A. (1999). "Molecular simulation of the Joule-Thomson inversion curve of carbon dioxide", *Fluid Phase Equil.*, **165**, 147.

[11] Johnson, J. K., Zollweg, J. A. and Gubbins, K. E. (1993). "The Lennard-Jones equation of state revisited", *Molec. Phys.*, **78**, 591.

[12] Ferrenberg, A. M. and Swendsen, R. H. (1989). "Optimized Monte Carlo data analysis", *Phys. Rev. Lett.*, **63**, 1195.

[13] Hansmann, U. H. E. (1997). "Parallel tempering algorithm for conformational studies of biological molecules", *Chem. Phys. Lett.*, **281**, 140.

[14] Ortiz, W., Perlloni, A. and Lopez, G. E. (1998). "Extending the J-walking Monte Carlo algorithm to the isothermal–isobaric ensemble: solid–liquid equilibrium in clusters", *Chem. Phys. Lett.*, **298**, 66.

[15] Yan, Q. and de Pablo, J. J. (1999). "Hyper-parallel tempering Monte Carlo: Application to the Lennard-Jones fluid and restricted primitive model", *J. Chem. Phys.*, **111**, 9509.

[16] Allen, M. P. and Tildesley, D. J. (1987). *Computer Simulation of Liquids*, Oxford, New York.

[17] Ferrenberg, A. M. and Swendsen, R. H. (1988). "New Monte Carlo technique for studying phase transitions", *Phys. Rev. Lett.*, **61**, 2635.
[18] Escobedo, F. A. (1998). "Novel pseudo-ensembles for simulation of multicomponent phase equilibria" *J. Chem. Phys.*, **108**, 8761.
[19] Histogram reweighting is particularly effective when broad histograms can be generated, *e.g.*, close to a critical point.
[20] Such a dual approach is not unlike that used to compute heat capacities and enthalpies with a EoS; the EoS provides "departure functions" to correct the ideal gas properties.
[21] Reid, R. C., Prausnitz, J. M. and Poling, B. E. (1987). *The properties of gases and liquids*, McGraw Hill 4th edn., New York.
[22] Nath, S. K., Escobedo, F. A. and de Pablo, J. J. (1998). "On the simulation of vapor–liquid equilibria for alkanes", *J. Chem. Phys.*, **108**, 9905.
[23] Escobedo, F. A. (2000). "Molecular and Macroscopic Modeling of Phase Separation", *AIChE J.*, **46**, 2086.
[24] Jorgensen, W. L., Madura, J. D. and Swenson, C. J. (1984). *J. Am. Chem. Soc.*, **106**, 813.
[25] Rivera, J. L., Alejandre, J., Nath, S. K. and de Pablo, J. J. (2000). "Thermodynamic and transport properties of nitrogen and butane mixtures", *Molec. Phys.*, **98**, 43.
[26] The composition of this gas condensate is a simplified version of the mixture "GC4" used in Ref. [30] and originally reported by Asberg-Petersen, K. and Stenby, E. (1991). *Ind. Eng. Chem. Res.*, **30**, 248.
[27] Frenkel, D. and Smit, B. (1996). *Understanding Molecular Simulation*, Academic Press, San Diego.
[28] de Pablo, J. J., Laso, M. and Suter, U. W. (1992). "Simulation of polyethylene above and below the melting point", *J. Chem. Phys.*, **96**, 2395.
[29] Spyriouni, T., Economou, I. G. and Theodorou, D. N. (1998). "Phase equilibria of mixtures containing chain molecules predicted through a novel simulation scheme", *Phys. Rev. Lett.*, **80**, 4466.
[30] Kortekaas, W. G., Peters, C. J. and de Swaan Arons, J. (1997). "Joule-Thomson expansion of high-pressure high-temperature gas condensates", *Fluid Phase Equil.*, **139**, 205.
[31] A three-parameter EoS should be sufficiently flexible to locally fit the PVT surface.
[32] Amadei, A., Apol, M. E. F. and Berendsen, H. J. C. (1998). "On the use of quasi-Gaussian entropy theory in noncanonical ensembles. I. Prediction of temperature dependence of thermodynamic properties", *J. Chem. Phys.*, **109**, 3004.
[33] Apol, M. E. F., Amadei, A. and Berendsen, H. J. C. (1998). "On the use of quasi-Gaussian entropy theory in noncanonical ensembles. II. Prediction of density dependence of thermodynamic properties", *J. Chem. Phys.*, **109**, 3017.
[34] Kofke, D. A. (1993). "Direct evaluation of phase coexistence by molecular simulation *via* integration along the saturation line", *J. Chem. Phys.*, **98**, 4149.
[35] Coleman, T. C. and Stewart, R. B. (1971). "Thermodynamic properties of N_2 from 70 K to 1000 K with pressures up to 1000 atm", NAS-NRC 13th Int. Cong. of Refrigeration.
[36] Soave, G. (1972). "Equilibrium constants from a modified Redlich-Kwong equation of state", *Chem. Eng. Sci.*, **27**, 1197.
[37] Peng, D.-Y. and Robinson, D. B. (1976). "A new two-constant equation of state", *Ind. Eng. Chem. Fundam.*, **15**, 59.
[38] Amadei, A., Apol, M. E. F., Chillemi, G., Berendsen, H. J. C. and Di Nola, A. (1999). "Derivation of a general fluid equation of state based on the quasi-Gaussian entropy theory: application to the Lennard-Jones fluid", *Molec. Phys.*, **96**, 1469.
[39] Vargaftik, N. B. (1975). *Tables on the thermophysical properties of liquids and gases*, J. Wiley, New York.